Applied Thermal Engineering 230 (2023) 120638

Contents lists available at ScienceDirect

Applied Thermal Engineering

journal homepage: www.elsevier.com/locate/ate

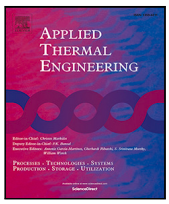

Research Paper

Two-stage multi-step energy model calibration of the cooling systems of a large-space commercial building

José Eduardo Pachano [a], María Fernández-Vigil Iglesias [a], Juan Carlos Saiz [b], Carlos Fernández Bandera [a,*]

[a] School of Architecture, University of Navarra, 31009 Pamplona, Spain
[b] Fundación Saltoki, Polígono Landaben Calle A, s/n., 31012 Pamplona, Spain

ARTICLE INFO

Keywords:
Building energy model (BEM)
HVAC
Calibration
Heat pump (HP)
Thermal energy simulation
Genetic algorithm

ABSTRACT

Buildings play a major role in energy expenditure, representing 40% of Europe's total energy consumption. It is estimated that heating, ventilation, and air conditioning systems consume between 50–60% of the total energy spent inside the building, thus corresponding to 20% of global worldwide energy consumption. Hence, there is a need to improve the accuracy of building thermal simulation and energy models that are essential in regulatory compliance calculations. In the present study, the authors empirically validate an optimization-based calibration methodology based on its application to a fully operational commercial building located in Pamplona, Navarre. The methodology used a white-box two-stage model in EnergyPlus, which combines a load profile object and a district cooling component to distribute the cooling load inside the building's thermal zones. The study optimized the parameters and performance curves of different cooling system components using a second-generation non-sorting genetic algorithm in jEPlus software and 985 h of ten-minute time-step data. Finally, a multi-level benchmark is executed, which evaluates the electric energy consumption of the building's heat pumps and the interior temperature of the different thermal zones for summer 2020 conditions. The assessment of the thermal and energy performance of the simulation model was conducted according to the requirements of the American Society of Heating, Refrigerating and Air-Conditioning Engineers, Guideline 14-2002, and the Chartered Institution of Building Services Engineers, Operation Performance Technical Memoranda 63.

1. Introduction

One of the main challenges in today's world is to optimize the use of resources and promote energy savings by minimizing energy consumption and CO_2 emissions in order to combat climate change. Buildings play a major role in this scenario. In Europe alone, their energy consumption represents 40% of the total, and they contribute to 36% of carbon dioxide emissions [1,2]. The latter shows an increasing trend that, if not addressed, is expected to increase by 40% by 2050 [3]. The fact is that heating, ventilation, and air conditioning (HVAC) systems play a major role in the energy consumption of buildings. In the case of Europe, the impact of heating and cooling energy consumption for conditioning indoor spaces is also estimated to surpass 60% of the total energy consumption in residential buildings and 45% in commercial buildings, with similar trends in the United States [4]. As a consequence, the European Union (EU) and governments around the world have established mandatory building energy studies and new energy saving policies for buildings and their conditioning systems aimed at responding to the current climate crisis [5]. To achieve this objective, the energy performance of the building and its different systems must be appropriately established to minimize the gap between the simulated environment results of building energy model (BEMs) and the measured reality. The use of BEMs that faithfully represent reality allows executing cost-effective analysis and accurately determining the thermal and energy performance of a building's different systems and equipment [6,7], predicting thermal comfort [8], developing energy conservation measures (ECMs) [9,10], optimizing HVAC configurations [11], studying renewable energy penetration or thermal mass activation [12], and implementing demand response (DR) [13,14] or model predictive control (MPC) [15,16] strategies, among others.

In order to minimize the gap between BEMs and reality, it is necessary to capture the building performance. To achieve this, the simulation model requires that the parameter values from the multiple

* Corresponding author.
E-mail addresses: jpachano@unav.es (J.E. Pachano), mfernandez-@unav.es (M. Fernández-Vigil Iglesias), jcsaiz@saltoki.es (J.C. Saiz), cfbandera@unav.es (C. Fernández Bandera).

https://doi.org/10.1016/j.applthermaleng.2023.120638
Received 31 May 2022; Received in revised form 14 April 2023; Accepted 22 April 2023
Available online 29 April 2023

systems that interact with the building's thermal energy balance be estimated [17]. Since this gap can be measured, several institutions have established procedures to benchmark the results of a BEM against actual readings, for example, the International Performance Measurement and Verification Protocol (IPMVP) [18], the American Society of Heating, Refrigerating and Air-Conditioning Engineers (ASHRAE) Guideline 14-2002 [19], the Chartered Institution of Building Services Engineers (CIBSE), Operation Performance TM-63 [20], and the Measure and Verification (M&V) Guidelines [21]. The present study uses IPMVP Option D, a non-intrusive tool that focuses on generating a calibrated BEM that is stable through time. It creates a building energy model inside a simulation environment that aims to accurately capture a building's thermal behavior and its energy performance [22–24].

There are many strategies to develop a calibrated BEM, with some studies using sensitivity analysis of parameters [25–27] while others apply a Bayesian approach [28–32], uncertainty analysis [33,34], goodness of fit [35], or even focus on the application of different optimization algorithms [24,36]. It is important to note that, in some studies, such as Aftab et al. [37], Chong and Menberg [30], Qiu et al. [36], and Yuan et al. [38], the process applied to the simulation model attempts to optimize multiple parameters, for both passive or active building systems, in simultaneous calibration. This approach may spread the error inside the simulation environment, generating a BEM that may be unfit for the study of certain ECMs. Hence, there is a need to separate the different building systems to minimize the spread of errors and to subdivide the systems by seasonal performance, treating heating and cooling systems independently, as suggested by Guyot et al. [39]. Moreover, since the building demand is closely related to the energy loss and gains through the envelope system (Annex 49 [40,41]), some studies have taken a multi-step approach that addresses the envelope before optimizing HVAC parameter values [42–47], which prevents the error spreading to the HVAC system from the envelope.

In terms of HVAC parameter calibration, some studies such as Hydeman et al. [48,49] focus on obtaining the equipment performance curves to match the BEM's energy outputs. Yin et al. [50] used indoor set-points to determine the building's consumption, whereas Kim et al. [45] use outdoor set-points to find a solution. Other studies add parameters related to electric energy efficiency related, such as the coefficient of performance (COP), to the use of such set-points to achieve energy calibration [30,32,51,52]. However, using set-points as key variable parameters may limit the use of the BEM and render it unusable for energy saving strategies based on the use of such set-point optimization. That is the reason why studies such as Yuan et al. [38] focused on efficiency-related parameters such as COP and air flow to obtain the building's energy consumption. For most cases, however, the performed calibration focuses on a single energy benchmark process: either energy performance or indoor comfort. The fact is that when improving the results of energy consumption in a given BEM, the impact on the thermal behavior of the model's indoor spaces should also take into account.

Therefore, to achieve a BEM that truly captures the building performance and its HVAC system, a multi-level benchmark must be used. In other words, both energy consumption and indoor climate must meet calibration criteria in resolution of the same time step [43,44,53]. This presents the challenge of addressing the uncertainties of the energy distribution system in an actual in-operation test site [46]. The division of the BEM into two stages, by the use of a load profile [31] in conjunction with a district cooling object that represents exact cooling energy provided to the building, is a strategy that allows distributing cooling energy into multiple systems and their TZ.

The novelty of the present study is its focus on empirically validating the multi-step methodology used by Pachano et al. [53], which generated positive results when calibrating an HVAC system under winter conditions, and applying it now to a completely different HVAC set-up that operates during summer. The generated physics-based model describes the building and its HVAC equipment in detail, it is a simulation model that represents the nonlinear dynamic system (NDS) between the building behavior and its HVAC control operation [54,55]. The study uses a multi-objective non-sorting genetic algorithm (NSGA-II) for optimizing the values of different HVAC performance parameters that intervene in the NDS in order to find a solution to the inherent nonlinearities in the thermal transfer phenomena, resulting on the empirical calibration of the HVAC components introduced in the BEM.

To achieve this, the 2020 summer measurement campaign is used, relying on minimum sensor deployment inside the building and supported by data obtained from the building management system (BMS) to establish HVAC operation. The main challenge in this approach relies in distributing the energy to the different terminal units in the building when the thermal carrier fluid flow on each of the different distribution pipelines is unknown. By making use of EnergyPlus load profile and district cooling components, the building's measured cooling consumption works as a pivot, or link, to generate this white-box two-stage BEM. This allows the calibration of parameter values and performance curves for the production heat pump (HP) group and the different terminal units (chilled water storage, air handling unit, cooling coil, and chilled beams) installed inside a real test site commercial building located in Pamplona, Navarre, under normal day-to-day operation. The resulting white-box two-stage BEM complies to international standards in both hourly electric energy consumption and indoor temperatures and allows the assessment of both production units and demand side terminal units. The BEM reaches calibration status using only 985 h of ten-minute time-step data and remains stable during the next 690 h of previously unseen data used as a validation period.

The paper is structured as follows: Section 2 describes the calibration methodology that is applied to the building and its HVAC systems. Section 3 briefly states how the baseline BEM is generated and it indicates the building configuration and HVAC equipment and includes data quality considerations used in the process. Section 4 states and discuss the results obtained during the BEM training and checking periods, comparing the calibrated BEM results with those obtained from a state-of-the-art baseline BEM. It illustrates the benefits of using the building demand as a link between production units and the building's terminal units. Finally, Section 5 presents the conclusions reached in this study and lists future applications for calibrated BEMs.

2. Calibration process

2.1. Methodology

The inverse calibration process applied in this study has been empirically validated, with successful results, in our previous works [53,56]. The following section briefly describes the overall process applied in this study.

As shown in Fig. 1, this process aims to generate a calibrated BEM that captures the behavior of the building thermodynamics and the installed HVAC system. To achieve this, data are gathered from the test site and classified as either input data, to stress the simulation, or control data, for benchmark purposes. The gathered data undergo an evaluation process to clean the stream from blank or error values. Table 1 displays the type of sensors deployed in the site for calibration purposes.

A baseline model is generated in the EnergyPlus [57] white-box simulation environment containing the available input data, weather conditions, and stressing factors; with the aim of representing the real conditions of the site as accurately as possible [44]. The methodology explained by Ramos et al. [24] and validated by Gutierrez et al. [56] is thus applied: The first key step of the process is to undergo separate calibration of the BEM's envelope in order to minimize the error produced by this system and accurately establish the building's heating and cooling demand (Annex 49 [40,41]). Since indoor temperatures are

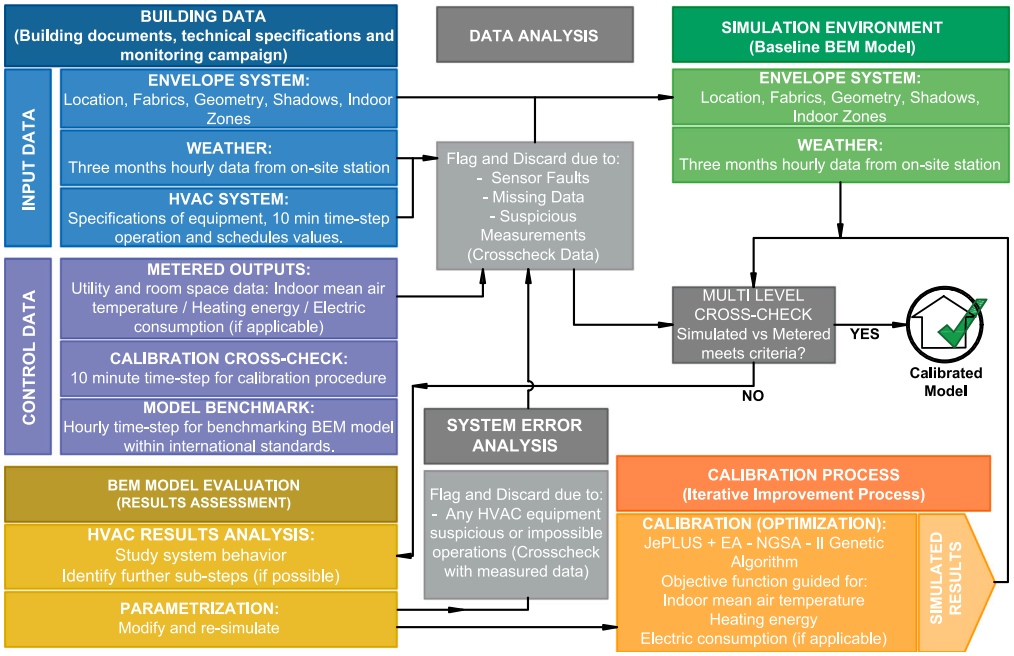

Fig. 1. Overview of the inverse calibration process applied in this study. The process has been expanded to add additional data analysis from previous work (Pachano et al. [53]).

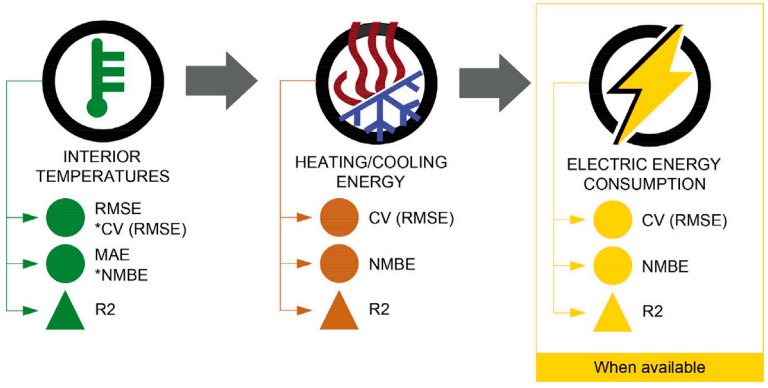

Fig. 2. Conditions required for the Calibration process. Simulated results must fit with all levels.
(Note*: The NMBE and CV(RMSE) indices for indoor temperature are only displayed to execute comparisons with existing literature.).

Table 1
List of measurements used in the test site data driven BEM building and HVAC system.

Measurement	Units
Weather :	
Outdoor Dry Bulb Temperature	°C
Outdoor Relative Humidity	%
Diffuse Radiation	W/m^2
Global Horizontal Radiation	W/m^2
Atmospheric Pressure	Pa
Wind Direction	deg
Wind Speed	m/s
Precipitation	mm
IndoorClimate :	
Indoor Room Temperature	°C
HVACSystem :	
Equipment ON/OFF status	1/0
Equipment Temperature Set-Points	°C
Equipment Flow Rates	m^3/s
ElectricConsumption :	
HVAC Electric Energy Consumption	Wh
HVAC Electric Power Rate Consumption	W

correlated with HVAC performance and consumption, this step makes the future assessment of the building HVAC system possible.

Once this is achieved, equipment values are parameterized and an iterative optimization process begins, shifting their values with the help of a second generation multi-objective non-sorting genetic algorithm (NSGA-II) applied by jEPlus+EA software [58,59]. This process is performed separately for heating and cooling conditions, and this seasonal division reduces the number of involved parameters and the size of search space under analysis. The resulting selected key parameters are tabulated in Section 4.3.

To guide the optimization process, a multi-level objective function is introduced. As stated in Fig. 2, this objective function aims to find the best possible solution for the parameter values based on multi-level comparison of simulated results with measured data until it meets the international standard criteria for indoor building temperatures, heating production energy, and electric consumption.

The applied methodology requires a large amount of data from multiple sensors inside the building to stress and describe the operation of the building's multiple systems. Since it attempts to calibrate the simulation model with a shorter time lapse than the one suggested by ASHRAE Guidelines 14, it requires short time-steps spanning from 10 to 15 minutes. Hence, the data used inside this process must undergo

Table 2
Calibration threshold values for uncertainty hourly error indices.

Hourly Index	Energy Consumption		Indoor Temperature
	ASHRAE	IPMVP	CIBSE VDI-6020
MAE (°C)	—	—	≤ 2.0
RMSE (°C)	—	—	≤ 1.5
NMBE (%)	≤ ± 10	≤ ± 5	—
CV(RMSE) (%)	≤ 30	≤ 20	—
R^2 (%)	≥ 75	≥ 75	≥ 75

exhaustive analysis and filtering prior to use. Additionally, the technology used in this calibration process is limited to the quality and detail of the building's system information and component specifications, particularly when developing the baseline model, which tries to represent the actual HVAC system deployed inside the building as faithfully as possible.

2.2. Calibration threshold indices

For a BEM to be considered calibrated, the simulated results for indoor temperature and energy consumption must reach a threshold set by international standards. In terms of energy performance, the BEM must meet the requirements of either ASHRAE Guideline 14 [19] or IPMVP [18]. For indoor temperature performance, the model must meet the threshold suggested by the CIBSE, Operation Performance TM-63 [20], and the German standard VDI-6020:2002 [60].

Table 2 shows the index threshold the BEM results must meet to achieve calibration. These limit values have been established for a continuous stream of yearly data. However, one big challenge faced when working in test sites that are actively in operation is to obtain such continuous flow of data. One of the aims of this study is to achieve BEM calibration using less data than the yearly stream suggested by international protocols and validate the model stability through a checking period characterized by the use of previously unseen data to stress the model.

The bias indices used in the benchmark process between the BEM simulated results and measured on-site readings are the mean absolute error (MAE) shown in Eq. (1), the normalized mean bias error (NMBE) shown in Eq. (2), the root mean square error (RMSE) displayed in Eq. (3), and the coefficient of variation of the root mean square error (CVRMSE) shown in Eq. (4). It is important to note that although use of the square of the Pearson correlation coefficient (R^2) shown in Eq. (5) is recommended in both ASHRAE Guideline 14 [19] and IPMVP [18], using this goodness-of-fit coefficient in conjunction with a bias index allows us to assess how well the BEM fits in reality [61], which is why it is also used for temperature assessment.

$$MAE = \frac{\sum_{i=1}^{n} |m_i - s_i|}{n}, \tag{1}$$

$$NMBE = \frac{1}{\overline{m}} \cdot \frac{\sum_{i=1}^{n} (m_i - s_i)}{n - p} .100(\%) \tag{2}$$

$$RMSE = \sqrt{\frac{\sum_{i=1}^{n} (m_i - s_i)^2}{n}} \tag{3}$$

$$CV(RMSE) = \frac{1}{\overline{m}} \cdot \sqrt{\frac{\sum_{i=1}^{n} (m_i - s_i)^2}{n - p}} .100(\%) \tag{4}$$

$$R^2 = \left(\frac{\sum_{i=1}^{n} (m_i - \overline{m}).(s_i - \overline{s})}{\sqrt{\sum_{i=1}^{n} (m_i - \overline{m})^2 . \sum_{i=1}^{n} (s_i - \overline{s})^2}} \right)^2 \tag{5}$$

3. Test site description

Located at 407 meters above sea level, in Pamplona, Spain, the selected test site operates as a commercial business and product showcase center. It is part of an industrial park dedicated to the sale and manufacture of construction materials run by a Spanish company. Pamplona has a temperate climate characterized by significant rainfall, which reaches an annual of 784 mm with precipitation even in its driest months and no significant difference in precipitation between seasons. The climate is characterized by an average annual temperature of 11.3 °C, with the maximum average reaching 19.4 °C in August and minimum average of 3.9 °C in January. According to the Köppen Climate Classification, it is defined as a temperate oceanic climate or Cfb. This climate is dominated by the polar front and oceanic currents, producing frequently changeable and overcast weather [62].

Weather plays a major role when developing a calibrated BEM. Working in conjunction with indoor comfort conditions, it is one of the main stress factors for the building [63]. In fact, on-site weather is correlated with both the actual building energy demand and the performance of its installed HVAC equipment [64,65]. For these reasons, an on-site weather station has been installed on the roof of the test site building. The station comprises of a HOBO RX3000 data logger with wireless internet connection, and details of the accuracy and range of the sensors deployed in the weather station are listed in Table 3.

3.1. Building characteristics

The building displayed in Fig. 3 is a three-story industrial warehouse of 9,366.74 m^2, and it has been refurbished for commercial purposes. The basement holds changing rooms, lockers, and seminars for training purposes. The ground floor is divided by its occupational use into store and sales offices, which are conditioned, and storage spaces. On the first floor, a large conditioned area is used for product showcasing, with project offices placed in the southwest corner. On the third floor, a small space that rises on the northeast corner houses the only HVAC service room.

According to as-built technical documents, the building's structure comprises a steel framework expansion constructed over the old industrial concrete block. The newly built envelope on its upper floors and southern facade mainly consist of large double glazing windows set on aluminum frames with thermal bridge disruption (thermal transmittance "U" value range of 1.351–1.422 W/m^2K). The new north side opaque facade is composed of an 8 cm composite steel panel with 25 cm of rockwool insulation and an interior 3 cm gypsum panel (U value = 0.105 W/m^2K). The ground floor facade retains the building's original on-site manufactured double glazing (U value = 2.800 W/m^2K), and the original masonry construction comprises 29 cm of double ceramic blocks, a 2 cm air cavity as insulation, and 3 cm sleet of gypsum as an internal finish (U value = 0.924 W/m^2K). Finally, the building's roof is composed of a composite 10 cm steel deck (U value = 0.374 W/m^2K), and the exposed first floor projection is a 67 cm light concrete slab (U value = 1.535 W/m^2K).

3.2. Building's HVAC system

The geometry of the different thermal zones (TZs) in the building is characterized by large open spaces with smaller isolated rooms dedicated to serve as offices. The layout requires the use of multiple independent systems to maintain interior climate temperature on each one of the conditioned spaces. The main HVAC system comprises one hot/chilled water based system supported by an air handling unit (AHU). The purpose of this system is to maintain indoor temperatures in the large spaces of the ground floor main store (TZ-44 and TZ-45), sales offices (TZ-36 to 40) and on the first floor showcase center (TZ-07, TZ-08 and TZ-09). Because the present study focuses on summer conditions, the areas displayed in Table 4 are those that are conditioned

Fig. 3. Left: Photograph of the commercial test site located in Pamplona, Spain (source: Roberto Lechado). Right: Baseline BEM generated by DesignBuilderV6 software.

Table 3
Weather station sensors and accuracy values for the test site.

toprule Sensor	Units	Range	Resolution	Accuracy
Temperature	°C	−40º to +65º	± 0.1	± 0.5
Humidity	%	0 to 100	± 1.0	± 3.0% (0-90) ± 4.0% (90–100)
Global Solar Radiation	W/m^2	0 to 1500	1	≤ 10
Diffuse Solar Radiation	W/m^2	0 to 1500	1	≤ 20
Wind Speed	m/s	1 to 67	0.44	± 1/± 5%
Wind Direction	º	1 to 360	1.0	± 4%
Precipitation	mm	—	0.2	± 4%/0.25 (≤ 50 mm) ± 5%/0.25 (≥ 50 mm)
Atmospheric Pressure	mbar	880 to 1080	± 0.1	± 1

Table 4
The effective floor area and indoor air volume of thermal zones in the conditioned building.

	TZ07	TZ08	TZ09	TZ44	TZ45
Area (m^2)	1,296.42	947.74	1,786.38	875.34	829.53
Volume (m^3)	7,889.12	5,746.42	11,583.38	4,293.66	4,093.64

exclusively by the chilled water HVAC system. This system provides cooling to an air volume of 3,606.22 m^3, which represents 61.23% of the whole building. The remaining 38.77% belongs to TZs that are either conditioned by secondary four-pipe multi-split variable refrigerant flow (VRF), which is outside the scope of this study, or to unconditioned areas. In both cases, an ideal load system has been introduced inside the BEM. This component fixes the TZ interior temperature to the values obtained from the building's sensors in order to introduce their actual thermal behavior and reduce the uncertainty produced because of any adjacent heat transfer.

The main system process and identification diagram (P&ID) displayed in Fig. 4 allows for seasonal changes between winter and summer operation. The production systems comprise a pre-installed boiler packet group of 330 kW with three 110 kW condensing boilers set up in cascade (which are not part of the scope of the present study), and a heat pump (HP) group set in a similar array with four HP with a heating/cooling capacity of 87.7/72.6 kW each supported by a 1500 L buffer tank. Although the described system allows the operation of the boiler group in conjunction with the HP group, the building management system (BMS) restricts the HP group for operating during winter, turning this production system on solely during summer when the boilers are turned off.

During summer, the valves are operated in a way that chilled water flows directly from the HP group into both the buffer tank and the six pipelines of the distribution system. As displayed in Fig. 4, the building endpoint systems are, from left to right, wall-mounted waterboard radiators (operating solely during winter and therefore not part of the scope of this study), ceiling radiator panels that also work as chilled beams during summer installed in the ground floor store (TZ-44 and TZ-45) and in the first floor showcase center (TZ-07, TZ-08 and TZ-09), and the cooling coil of the AHU, which delivers air into the first floor showcase center (TZ-07, TZ-08 and TZ-09).

The showcase center's AHU has a rotary air-to-air heat exchanger with a nominal capacity of 50,000 m^3/h supply air fan, and a similar exchanger for returning air, which is collected from the northeast corner of the building (TZ-07).

3.3. Baseline BEM considerations

The TZ division conducted when the baseline BEM that was generated, takes into account the HVAC distribution system and the type of end point systems that are located across the building. The large open spaces were divided in several TZs, such as the ground floor store, which was split in two TZs, and the first floor showcase center, divided into three separate TZs, each holding its own HVAC branch and the end point system. The division wall used in the simulation environment is a thin high conductive shell that allows temperature transfer between the adjacent zones. To emulate the air convection produced by AHU operation in the first floor TZ, an air mixing object was introduced between TZ-07, −08, and −09, and its parameter value was set to be optimized by the calibration process.

The detailed HVAC system illustrated in Fig. 5 is the result of translating the building's HVAC P&ID shown in Fig. 4 into an EnergyPlus simulation environment. Using DesignBuilderV6 software, the different HVAC systems are set up inside the BEM, their nodes connected to the different TZs, and their component values set according to the those obtained from the building's technical documents. The objective is to create a baseline BEM that closely resembles reality. Once the model is complete, input data obtained from sensors and the building management system (BMS) are introduced into the model for stressing purposes, and the calibration process can begin.

As displayed in Fig. 5, the resulting baseline BEM has two main loops, a heating and a cooling loop, supported by an auxiliary air handling unit loop that intervene whenever the building demands thermal energy. The icons in the figure stand for key nodes that intervene in the process. Those labeled as "T" stand for the indoor temperature sensors, "H" indicates the location of the thermal energy meter located in the heating and cooling production pipes, and "E" indicates the electric energy meter sensors of the heat pumps (HPs).

3.3.1. Heating loop

The heating loop is subdivided into heating production, piping distribution ring, and terminal units inside the building's TZs. It has been modeled for future use, because it is outside the scope of the current study, and the system has been turned off.

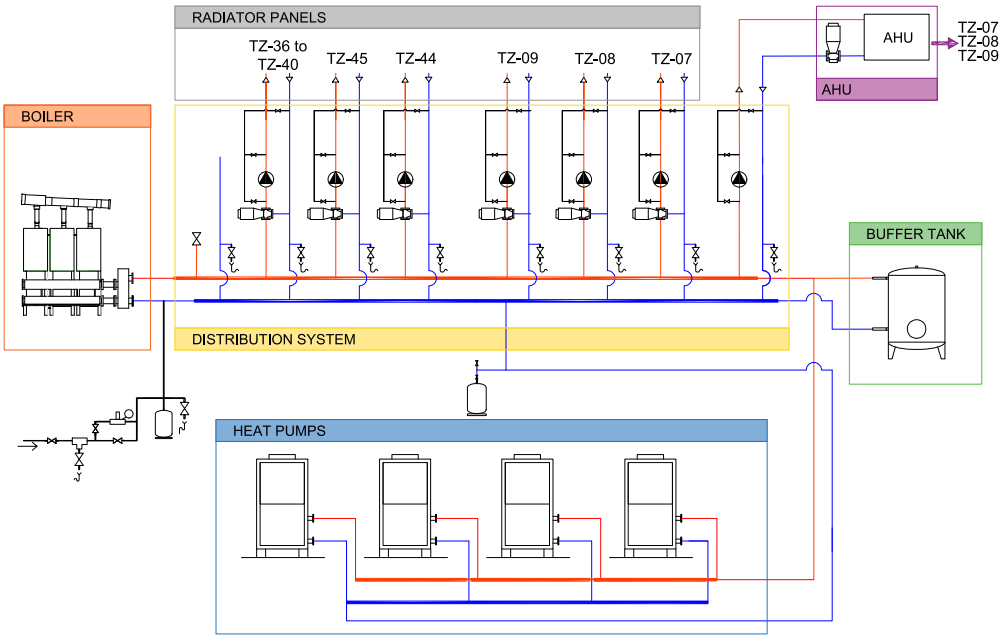

Fig. 4. Overview of the water-based HVAC boiler and heat pump installation diagram.

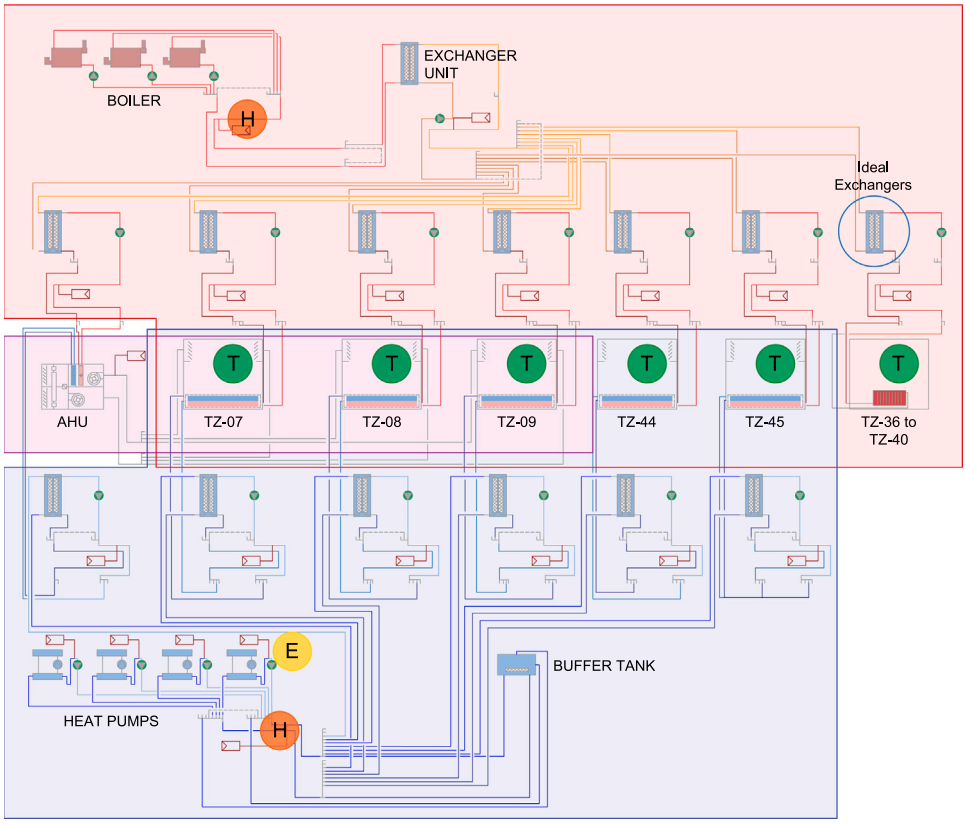

Fig. 5. Overview of the test site HVAC simulation environment.

3.3.2. Cooling loop

As with the heating loop, the cooling loop is subdivided into cooling production, distribution ring, and terminal units. Here, the heat pumps, modeled as air-to-water electric chillers, because they solely respond to cooling demand, are set in cascade to operate ruled by a fixed set-point on each unit (HP01 10.0 °C, HP-02 10.5 °C, HP-03 11.0 °C, and HP-04 11.5 °C). These units provide chilled water to both the building and the buffer tank. Therefore, the buffer tank is set to work in parallel with the production components as shown in Fig. 4, providing chilled water into the building and acting as a damper that increases the system inertia. The cooling distribution ring has three-way valves on each branch that are modeled as an ideal fluid-to-fluid heat exchanger and connected to the terminal units in the building. Because the valve that delivers water to the wall-mounted radiators in the offices is closed during summer,

it is not introduced in the current study. The scope focuses only on the branches belonging to the AHU cooling coil and the chilled beams defined as low temperature radiant surfaces on the ceiling of the ground floor store (TZ-44 and −45) and the first floor showcase center (TZ-07, −08, and −09) [57].

Fixing the simulated temperature set-point values for both indoor spaces and the different system branches with the value requested by the BMS will allow the calibration process to focus on the performance of each individual component. The calibration will proceed to vary the different parameter values of the components involved in the production and delivery of heating/cooling into building spaces. As a result, it will find the optimized parameter values that, under particular fixed set-point conditions, will result in the simulation model closely matching the thermal behavior of the real building and the electric consumption of its HVAC equipment. The multi-level benchmark introduced in the process allows capturing the performance of each of the different HVAC components and achieving fairly accurate calculations for optimized distribution of the produced cooling energy delivered into the different TZs. The resulting model retains its flexibility; in other words, it can be used to develop energy saving strategies that require set-point optimization, such as demand control (DC), thermal mass activation, or model predictive control (MPC).

The splitter component located after the chillers serves as the link between the production system and the distribution system. Here, the model can be separated into multiple steps to save computational resources [66]. By using a data-driven load profile [31], the calibration process can first focus on centering the value range of the chillers' parameter values, including those belonging to the equipment performance curves. These curves are defined inside the baseline BEM by following the least-squares linear regression method stated by Hydeman et al. [48,49] that links the performance of the equipment to both indoor and outdoor climate by establishing the coefficients C_i shown in Eq. (6).

$$z = C_1 + C_2 * x + C_3 * x^2 + C_4 * y + C_5 * y^2 + C_6 * x * y, \quad (6)$$

Once this is achieved, the load profile element is removed, the chillers are turned off, and a district cooling element is introduced on the supply side. By setting the district cooling to match the cooling demand used in the load profile, we effectively cap the maximum available cooling production. Because the cooling energy available is now limited, we can perform the calibration of parameters for the terminal units and thus generated this white-box two-stage BEM. Here, the radiant surfaces are clustered into three typical groups based on the building's documents and visual inspection to reduce the search space, and a new calibration process takes place. This step aims to focus on centering the values of the distribution system and the terminal unit parameters. The objective here is to find the best possible distribution of the energy to different branches by consuming all of the energy provided by the district cooling element while maintaining the indoor temperature in each TZ.

3.3.3. Auxiliary air handling unit loop

The purpose of this system is to deliver heating, cooling, and ventilation exclusively to the showcase center located on the first floor. This loop is connected to the different building spaces using variable air volume terminal units with no reheating elements. This allows the use of variable speed fans inside the AHU, and a single set-point is introduced on the air outlet node to control the temperature of the supplied air flow. As such, the AHU modeled inside EnergyPlus emulates its installed counterpart, an encased factory-made assembly package [67]. The unit allows outdoor air supply, sensible and latent heat recovery, and TZ air recirculation and mixing and provides thermal comfort air into the spaces by operating a mutually exclusive pair of water-to-air heating and cooling coils [57].

3.3.4. Occupation and internal loads

The areas belonging to the ground floor store (TZ-44 and −45) are occupied by two permanent cashier operators and auxiliary personnel. The areas of the exposition center (TZ-07, −08, and −09) have 18 permanent office workers. Even if the permanent occupation density is minimum, given the large air volume of the indoor spaces, the present study collects the thermal information from the occupation and equipment loads in the indoor temperature data stream. While the calibration of the building's envelope is performed during free oscillation periods, where there is no occupancy, the calibration of the cooling systems makes use of this temperature data file for continuous benchmarking of simulated results. This introduces the effects produced by the occupation load into the optimization of parameter values.

3.4. Data classification, analysis, and deployment

As mention in our previous work [53], data have been collected from multiple sources and introduced inside the simulation environment following the quality guidelines and ranking criteria that structure data from best-to-worst quality source [68–71]. The objective is to prioritize the use of data collected from the BMS system in conjunction with different sensors deployed inside the building and its HVAC systems over data from the site technical documents, commercial brochures, or experience.

The resulting BEM employs input data, used to constrain and stress the BEM (on-site weather, on/off schedules, set-points, and baseline parameter values), and control data, used to perform benchmarking of the BEM (indoor temperatures, thermal energy production, and electric energy consumption). This process allows estimating how the consumed energy has been distributed across the different simulated spaces.

The measured data undergo a validation process. The first step is to check the health of the data stream, wherein the time-step values are checked for any blanks or out of range values. As general rule, when there is a data gap bigger than 3 h or a value out of range, the data are filled by linear interpolation between two known values and flagged as not valid for the calibration process. For gaps under this threshold, the same principle for filling the data are applied, but they are only flagged with a warning, and the process continues.

During this process, data are crosschecked between different sensors belonging to the building and HVAC systems in order to understand the HVAC behavior [72], find correlations between the different components of the equipment and the building, and verify the correct operation of the HVAC system. This in-depth analysis of the data allows to clean the stream from sensor and equipment malfunctions prior the calibration process. Because data are key in developing the BEM, the continuous assessment of their quality becomes critical. This requires clear communication between the data analyst and the building maintenance personnel to examine faulty events, perform any on-site solution if needed, and minimize their occurrence.

As a result, a total of 5911 ten-minute time-steps (985.16 h) between June and August 2020 were used to perform the calibration process. Although this reduced amount of viable data indicates how difficult is to obtain clean valid data from a commercial building in operation, it is also aligned with one of the objectives of this study: to achieve the best possible results using as much available data as possible.

4. Analysis of results and discussions

4.1. Production units: Calibration process

The selected calibration period runs from the 1st of June until the 15th of August 2020, as shown in Table 5. This time period coincides with the building's HVAC system being set in cooling mode and is characterized by an average outdoor temperature of 20.814 °C,

Table 5
On-site summer training period weather details from June 2020 to the 15th of August 2020.

Description		Units	Training period			
			Jun	Jul	Aug	Average
Outdoor Dry Bulb Temperature	Average	°C	19.480	21.050	21.913	20.814
	Maximum	°C	36.600	41.700	42.500	40.267
	Minimum	°C	8.100	10.300	10.200	9.533
Global Radiation	Average	W/m^2	347.466	369.141	399.895	372.167
Diffuse Radiation	Average	W/m^2	40.845	34.398	44.103	39.782

with maximum temperatures reaching above 40 °C during building operational hours.

The first step of the calibration process focuses on establishing the parameter values of the HP group, that is for the master unit and its three slave units (HP-Master 00 and HP-Slave 01 to 03). By applying the load profile object, the building and its terminal units are disconnected from the production systems and replaced by the exact cooling demand requested by them. This allows the calibration of the performance parameters and curve values that will allow fitting of the simulated electric consumption with the measured consumption. Table 6 displays the final parameter values obtained from this process.

A key parameter in this optimization was the load distribution scheme, because it establishes how the HP group operates in order to meet the load demand. The installed units start-up logic is currently constrained by temperature such that they operate only based on chilled water set-point, causing the master unit to deliver water at 10 °C, and the slave units at 10.5, 11, and 11.5 °C each. This is the reason why the load distribution scheme was parameterized to the available options in EnergyPlus, allowing the optimization process to select the scheme that best fits the electric consumption. Since these distribution schemes intimately work with the equipment's part load ratio (PLR), a family of PLR curves was generated to find the one that fits best. The obtained solution operates each HP unit at its "optimal" PLR, and the remaining cooling demand is distributed evenly to all the other components [57]. The obtained PLR curves are shown in Table 7 and Fig. 6.

The results in Table 6 show that the HP-Master 00 and the HP-slave 01 have a reduced cooling capacity (83.3% and 90.7% of their nominal value) and yet their coefficient of performance (COP) is similar to the that obtained for the baseline BEM. In the case of HP-Slave 02, although the cooling capacity follows this trend, its COP drops 35%. The HP-Slave 04 has a cooling capacity above the unit's nominal value accompanied with a COP drop of 13%. There may be two main reasons

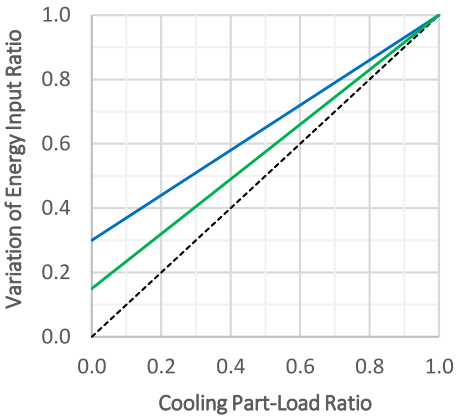

Fig. 6. Generated PLR curves displayed in black for the baseline BEM and in blue (HP-Master 00) and green (HP-Slave) for the calibrated BEM.

for these results. First, the load distribution scheme ensures that after unit 00, unit 01 is the unit that is mostly active, resulting in the slave unit working in far more time-steps than for unit 02 or 03. Second, the curve parameters were grouped to perform the optimization clusters for all slave units under the same curve, and thus unit 02 and 03 parameter values adapted based on a curve that fits mostly to the operation of unit 01.

The optimized curve coefficient values for the HP-Master 00 and HP-Slave units 01–03 is displayed on Table 7. Although it is possible to assign individual curves to each unit, allowing us to fine-tune the system, each set of curves requires growth of the parameter tree by the addition of 16 genes, which in turn increases the search space exponentially if each gene holds 10 or more discrete values.

When the curves are plotted, as shown in Fig. 7, it is clear that there is a slight reduction in the performance for all the HP units in terms of cooling capacity. However, in terms of the electric input ratio curve, there is a difference: the HP-Master 00 unit curve closely resembles the baseline BEM curve, the coefficients adapt to increase the performance under high outdoor temperatures (40 °C), whereas the curves for the HP slave group have an overall reduction of efficiency regardless of outdoor conditions.

The results from the calibration process are shown in Fig. 8, where a comparison between monthly and ten-minute time-step analysis can be viewed. In terms of monthly energy consumption, the baseline model closely resembles the electric measurements, maintaining its monthly

Table 6
Comparison of parameter values between the baseline BEM and calibrated BEM obtained after the calibration process of the heat pump group for the summer training period 2020.

Parameter	Units	Baseline BEM	Calibrated BEM			
Plant Loop Volume	L/s	1644	1534			
Load Dist. Scheme	—	SequentialLoad	Optimal			
			HP-Master 00	HP-Slave 01	HP-Slave 02	HP-Slave 03
Design Maximum Flow Rate	L/s	4.739	4.715	4.705	4.667	4.687
Motor Inefficiencies into Fluid Stream	—	0.000	0.587	0.767	0.480	0.814
Chiller Capacity	W	72600	60464	65867	63727	76275
Chiller COP	W/W	3.04	3.07	3.88	1.97	2.64
Chilled Water Temp.	C	7.000	6.653	6.798	6.964	6.594
Condenser Fluid Temp.	C	35.000	38.712	37.287	37.256	32.649
Chilled Water Flow Rate	L/s	3.472	4.857	3.834	3.541	4.427
Condenser Flow Rate	L/s	12500	10254	11845	10532	8301

Table 7
Comparison of curve values between the baseline BEM and calibrated BEM obtained after the calibration process of the heat pump group for the summer training period 2020.

Parameter	Units	Baseline BEM	Calibrated BEM	
			HP-Master 00	HP-Slave 01-03
Cooling Capacity Ratio Modifier Function of Temperature				
Coefficient C1	—	0.996439887	0.976632655	1.014602587
Coefficient C2	—	0.035830693	0.035375693	0.033003316
Coefficient C3	—	0.000400990	0.000386638	0.000350550
Coefficient C4	—	−0.004437624	−0.004327300	−0.004377654
Coefficient C5	—	−0.000027497	−0.000028809	−0.000026205
Coefficient C6	—	−0.000272673	−0.000267309	−0.000288703
Minimum Value of x	°C	5.560	5.466	6.068
Maximum Value of x	°C	10.000	9.649	9.083
Minimum Value of y	°C	23.890	19.740	21.744
Maximum Value of y	°C	46.110	42.079	40.509
Cooling Energy Input Ratio Modifier Function of Temperature				
Coefficient C1	—	0.738136935	0.723439808	0.650931546
Coefficient C2	—	−0.022575076	−0.023018375	−0.021865843
Coefficient C3	—	0.001045099	0.000943061	0.001006833
Coefficient C4	—	0.001149609	0.001084814	0.001233051
Coefficient C5	—	0.000359704	0.000393352	0.000378006
Coefficient C6	—	−0.000492416	−0.000498230	−0.000519527
Minimum Value of x	°C	5.560	5.466	6.068
Maximum Value of x	°C	10.000	9.649	9.083
Minimum Value of y	°C	23.890	19.740	21.744
Maximum Value of y	°C	46.110	42.079	40.509
Electric Input to Cooling Output Ratio Function of Part Load Ratio				
Coefficient C1	—	0.000	0.300	0.150
Coefficient C2	—	1.000	0.700	0.850
Coefficient C3	—	0.000	0.000	0.000

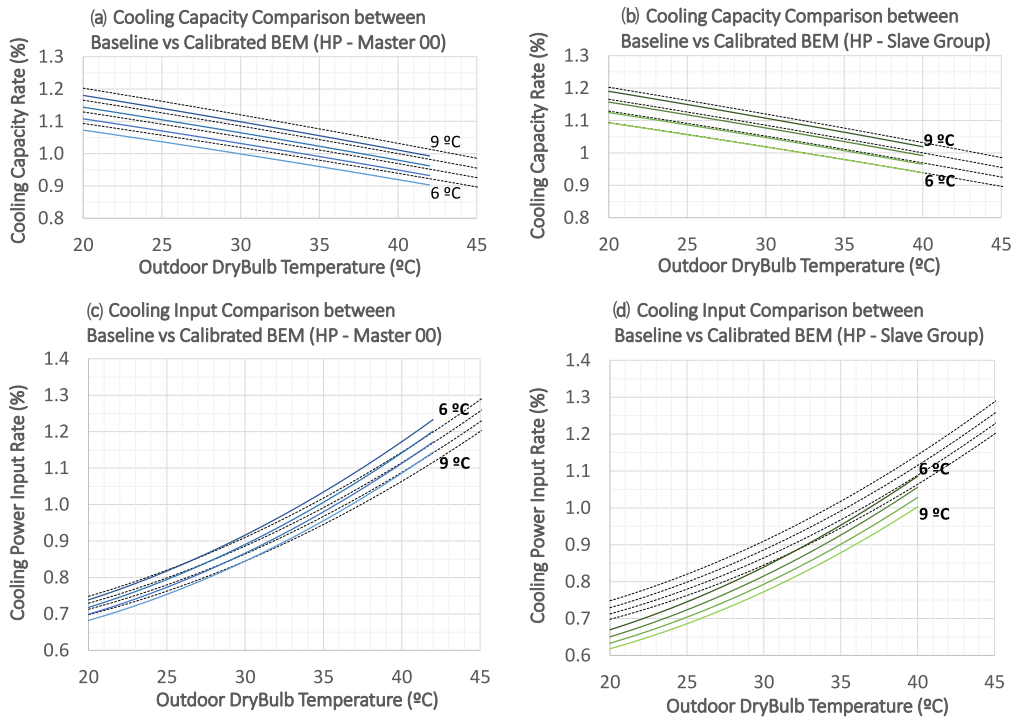

Fig. 7. Generated HP group performance curves displayed in black for the baseline BEM (technical documentation) and in blue (HP-Master 00) and green (HP-Slaves Group) for the calibrated BEM.

NMBE below 1%, but when assessed under a finer resolution, the baseline BEM fails to meet the criteria for hourly calibration. The dispersion graph shows how the calibration process aligns and clusters the time-step results along the ideal behavior diagonal line, generating a BEM that actually resembles how the equipment is operating at a detailed level.

This result becomes apparent when obtaining the uncertainty index for energy consumption, displayed in Table 8. The calibration process

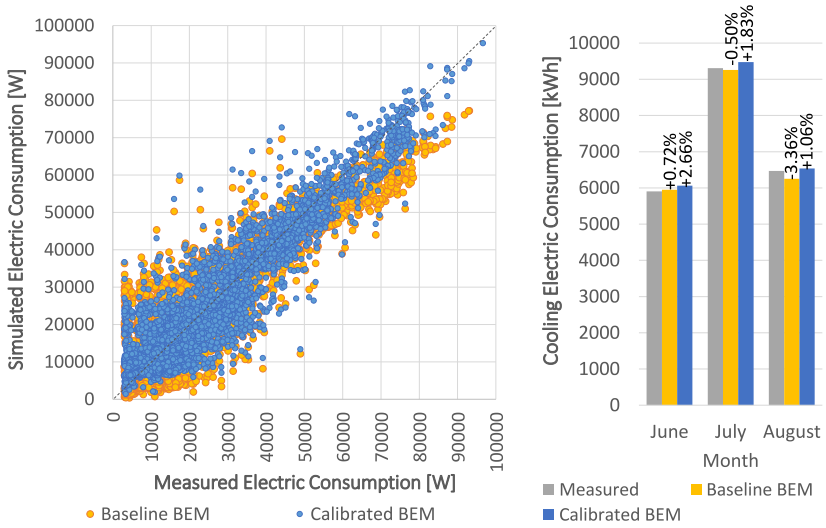

Fig. 8. Performance results for electric consumption of the calibrated BEM during the cooling calibration period from June 2020 to the 15th of August 2020.

Table 8
Electric consumption hourly uncertainty index for the cooling calibration period using 985.16 h of operation from June 2020 to the 15th of August 2020.

Index	International Standard		Electric Consumption Results	
	ASHRAE	IMPVP	Baseline Model	Calibrated Model
NMBE	±10%	±5%	0.969%	−1.704%
Cv(RMSE)	30%	20%	33.476%	28.451%
R^2[a]	75%	75%	82.271%	87.253%

[a]Although there is no universal standard for a minimum acceptable R^2 threshold, values above 75% are often considered a sign of a good causal relationship between the energy and independent variables [18].

manages to fit the model under international standards with 5% improvement in terms of the goodness-of-fit index. Moreover, it clearly shows why the use of multiple uncertainty indices is needed to validate a model, because the baseline BEM meets the hourly NMBE criteria but fails to meet the hourly Cv(RMSE).

The results of this first step pose an interesting question: To what degree does a model need to be calibrated? Whether to use the BEM at a broad resolution or fine-tune it to a minute-by-minute resolution will depend on the final purpose of the model. If it will be used for certification purposes or for establishing potential economical gains from certain refurbishments or energy conservation measures, then perhaps a monthly approach is sufficient. If dedicating the BEM to more precise tasks, however, such as predictive control, demand response, and fault detection diagnosis, the model is required to meet hourly criteria.

4.2. Demand side calibration process

The load profile object can be used as a pivot element between production systems and the building itself. Since it describes, in detail, the building's cooling demand based on measurements, it can also be introduced as a district cooling element inside the simulation environment. By introducing it as such, the demand side terminal units are limited to a maximum thermal energy delivery.

The fact is that besides fluid temperature and the pumps' nominal flow, established in technical documents, there is no water flow data stream for each one of the ramifications of the distribution system. Under this uncertainty, the parameters for maximum water flow in the variable speed pumps that belong to the distribution pipe system are set as variables to be optimized, as shown in Table 9. Because cooling production is limited by the district cooling object, the calibration process tries to find the solution that best fits indoor temperatures while consuming all of the delivered cooling energy.

This principle is applied for all terminal units, and the gene pool used has 93 parameters, each with 9 discrete values, that undergo calibration. The process is iterative, and once the best solution for the search space has been reached, the solution is studied, and a new set of discrete values is set in order to continue the process. When faced with a major uncertainty factor, such as the water flow for each distribution pipeline, the number of iterations increases. In the case of the demand side calibration, it took ten cycles to reach the solution, whereas in the case of the production systems, the solution was reached after three iterations.

The baseline BEM chilled beams were modeled based on blueprints, and their parameters set to catalog values. The installed system is complex and has multiple types of chilled water panels, with different sizes, geometry, and tubing. To reduce the search space, they are grouped according to thermal zone by the generated BEM, as shown in Table 10. Major changes in circuit and hydronic length as well as maximum water flow are observed in the obtained solution.

The baseline model air flow parameters were obtained from technical specifications and corrected based on measurements performed during the building inspection. During this measurement campaign, the AHU was set to deliver maximum air flow while measurements were taken downstream at the closest air outlets with the help of a hot wire anemometer rod. The acquisition of measurements proved challenging, given the height of the installation (over 6 m) and the impossibility to remove the air diffuser cap, which may take readings of air speed in a

Table 9
Comparison of parameter values between the baseline BEM and calibrated BEM obtained after the calibration process for the water distribution system (summer training period 2020).

Equipment/Component	Parameter	Units	Baseline BEM	Calibrated BEM
Water Based Distribution Loop System				
Chilled	Deadband Temperature Difference	ºC	2.000	0.186
Water	Uniform Skin Loss Coefficient	W/m^2	0.846	871.887
Storage	Use Side Heat Transfer Effectiveness	—	1.000	0.406
Tank	Use Side Design Flow Rate	L/s	17.825	10.162
	Source Side Heat Transfer Effectiveness	—	1.000	0.910
	Source Side Design Flow Rate	L/s	13.889	20.413
	Tank Recovery Time	hr	1.500	0.167
	Additional Destratification Conductivity	W/m	0.100	24.877
AHU Water	Design Maximum Flow Rate	L/s	10.929	13.966
Loop	Plant Loop Volume	m^3	0.340	0.323
TZ-07 Water	Design Maximum Flow Rate	L/s	1.293	1.059
Loop	Plant Loop Volume	m^3	0.771	0.818
TZ-08 Water	Design Maximum Flow Rate	L/s	0.921	0.855
Loop	Plant Loop Volume	m^3	0.575	0.519
TZ-09 Water	Design Maximum Flow Rate	L/s	1.778	1.453
Loop	Plant Loop Volume	m^3	1.541	1.443
TZ-44 Water	Design Maximum Flow Rate	L/s	1.000	1.330
Loop	Plant Loop Volume	m^3	0.539	0.569
TZ-45 Water	Design Maximum Flow Rate	L/s	1.282	1.352
Loop	Plant Loop Volume	m^3	0.574	0.568

Table 10
Comparison of parameter values between the baseline BEM and calibrated BEM obtained after the calibration process for chilled beams (summer training period 2020).

Equipment/Component	Parameter	Units	Baseline BEM	Calibrated BEM
Terminal Units: Water Based Radiator Panels (Chilled Beams)				
TZ-07	Tube Spacing	m	0.100	0.100
	Hydronic Tubing Outside Diameter	m	0.016	0.019
	Hydronic Tubing Length	m	1872.110	969.574
	Hydronic Tubing Conductivity	W/m-K	0.350	0.310
	Maximum Cold Water Flow	L/s	1.293	0.741
	Cooling Control Throttling Range	ºC	1.000	0.428
	Circuit Length	m	29.298	19.933
TZ-08	Tube Spacing	m	0.100	0.100
	Hydronic Tubing Outside Diameter	m	0.016	0.019
	Hydronic Tubing Length	m	1149.200	984.037
	Hydronic Tubing Conductivity	W/m-K	0.350	0.310
	Maximum Cold Water Flow	L/s	0.921	0.551
	Cooling Control Throttling Range	ºC	1.000	1.625
	Circuit Length	m	18.507	14.195
TZ-09	Tube Spacing	m	0.100	0.100
	Hydronic Tubing Outside Diameter	m	0.016	0.019
	Hydronic Tubing Length	m	2590.510	1754.257
	Hydronic Tubing Conductivity	W/m-K	0.350	0.310
	Maximum Cold Water Flow	L/s	1.778	2.314
	Cooling Control Throttling Range	ºC	1.000	0.307
	Circuit Length	m	44.711	21.084
TZ-44	Tube Spacing	m	0.100	0.100
	Hydronic Tubing Outside Diameter	m	0.016	0.009
	Hydronic Tubing Length	m	1184.000	539.482
	Hydronic Tubing Conductivity	W/m-K	0.350	0.371
	Maximum Cold Water Flow	L/s	1.000	0.803
	Cooling Control Throttling Range	ºC	1.000	1.015
	Circuit Length	m	24.667	17.424
TZ-45	Tube Spacing	m	0.100	0.076
	Hydronic Tubing Outside Diameter	m	0.016	0.009
	Hydronic Tubing Length	m	1202.680	882.669
	Hydronic Tubing Conductivity	W/m-K	0.350	0.371
	Maximum Cold Water Flow	L/s	1.282	1.106
	Cooling Control Throttling Range	ºC	1.000	1.007
	Circuit Length	m	12.528	12.831

turbulent flow. Because of these reasons, it is believed that the results from these measurements differ greatly from the maximum flow that the unit could provide (13.888 m^3/s), as shown in Table 11. Therefore, it was necessary to set these parameters inside the calibration. The results obtained for the calibrated BEM show that air flow values are close to the actual specified unit output (11.796 m^3/s or 84.9% of the

Table 11
Comparison of parameter values between the baseline BEM and calibrated BEM obtained after the calibration process for the air handling unit (summer training period 2020).

Component	Parameter	Units	Baseline BEM	Calibrated BEM
Air Handling Unit: Air Loop System				
AHU	Minimum Outdoor Air Flow Rate	L/s	2499.330	9568.476
	Maximum Outdoor Air Flow Rate	L/s	6652.301	11795.967
	Maximum Flow Rate	L/s	6652.301	11795.967
Supply Fan	Motor In Airstream Fraction		1.000	0.439
Extract Fan	Motor In Airstream Fraction		1.000	0.096
	Nominal Supply Air Flow Rate	L/s	5833.330	12567.670
Air to Air	Sensible Eff. at 100% Cooling Air Flow	—	0.711	0.673
Heat	Latent Eff. at 100% Cooling Air Flow	—	0.000	0.110
Exchanger	Sensible Eff. at 75% Cooling Air Flow	—	0.732	0.719
	Latent Eff. at 75% Cooling Air Flow	—	0.000	0.252
Terminal Units: Water Cooling Coil (AHU)				
Controller	Maximum Actuated Flow	L/s	11.940	5.533
Cooling	Design Water Flow Rate	L/s	11.940	8.281
Coil	Design Air Flow Rate	L/s	11666.670	7962.278
	Design Inlet Water Temperature	ºC	7.000	5.083
	Design Inlet Air Temperature	ºC	28.000	32.327
	Design Outlet Air Temperature	ºC	14.720	7.505
	Design Inlet Air Humidity Ratio	kgWater/kgDryAir	0.012	0.010
	Design Outlet Air Humidity Ratio	kgWater/kgDryAir	0.010	0.015

Table 12
Comparison of parameter values between the baseline BEM and calibrated BEM obtained after the calibration process for the air terminal units (summer training period 2020).

Equipment/Component	Parameter	Units	Baseline BEM	Calibrated BEM
Terminal Units: Air Terminals				
TZ-07	Maximum Air Flow Rate	L/s	1449.691	724.846
	Nominal Upstream Leakage Fraction	—	0.000	0.030
	Constant Downstream Leakage Fraction	—	0.000	0.199
TZ-08	Maximum Air Flow Rate	L/s	2815.080	745.233
	Nominal Upstream Leakage Fraction	—	0.000	0.128
	Constant Downstream Leakage Fraction	—	0.000	0.082
TZ-09	Maximum Air Flow Rate	L/s	2387.530	4470.000
	Nominal Upstream Leakage Fraction	—	0.000	0.035
	Constant Downstream Leakage Fraction	—	0.000	0.074
Zone Air Mixing				
TZ-07 to 09	Design Flow Rate	L/s	0.000	266.437
TZ-07 to 08	Design Flow Rate	L/s	0.000	338.366
TZ-08 to 07	Design Flow Rate	L/s	0.000	894.100
TZ-08 to 09	Design Flow Rate	L/s	0.000	1613.722
TZ-09 to 07	Design Flow Rate	L/s	0.000	0.000
TZ-09 to 08	Design Flow Rate	L/s	0.000	390.343

specified value), which better represent the equipment performance loss due to efficiency and operational hours.

Given the volume of the showcase floor, it was deemed necessary to subdivide it into three different TZs. The modeled TZs are separated by a high conductive partition that allows temperature exchange between the adjacent zones. However, the air recirculation duct of the air loop that delivers air into all of the showcase zones is located in the northeast corner of the building (TZ-07). In other words, when the AHU is operating, the supplied air generates a draft throughout the thermal zones. In order to model this behavior in a simplified way, a zone air mixing object was introduced, and the design flow rate between zones was parameterized, obtaining the results shown in Table 12.

With the generation and manipulation of a BEM, the aim is that it will resemble reality as much as possible. The parameters obtained as a solution satisfy indoor climate standards while consuming over 90% of the available cooling energy provided by the district cooling system. As shown in Fig. 9, if the system depletes district cooling, the dispersion graph would be a straight 45° line and, therefore, the model could be exclusively analyzed based on its indoor temperatures. The spread of dispersion points at high cooling demand rates, which can be seen in the figure, indicates that, at those corresponding times, indoor temperature has been reached using less thermal energy than what is available. The main reason for this behavior lies in the water flow distribution in each of the pipe branches. The calibration process tries to determine the maximum water flow for each, which allows the BEM to calculate the flow, between zero and this maximum value, based on the requested water set-point of the branch. The process tries to balance the thermal energy consumption while meeting the requirements for indoor temperature. This figure thus shows the results from trying to reach this equilibrium when the energy carrier flow on each branch is unknown.

When comparing the spread of baseline BEMs in Figs. 8 and 9, it appears that the production units have more favorable behavior, clustering around the ideal line, whereas terminal units on the demand side are unable to consume most of the available cooling energy. The separation of the model using the load profile/district cooling pivot show that the main potential challenge in this case lies in the demand side of the HVAC system. One of the reasons may be differences in

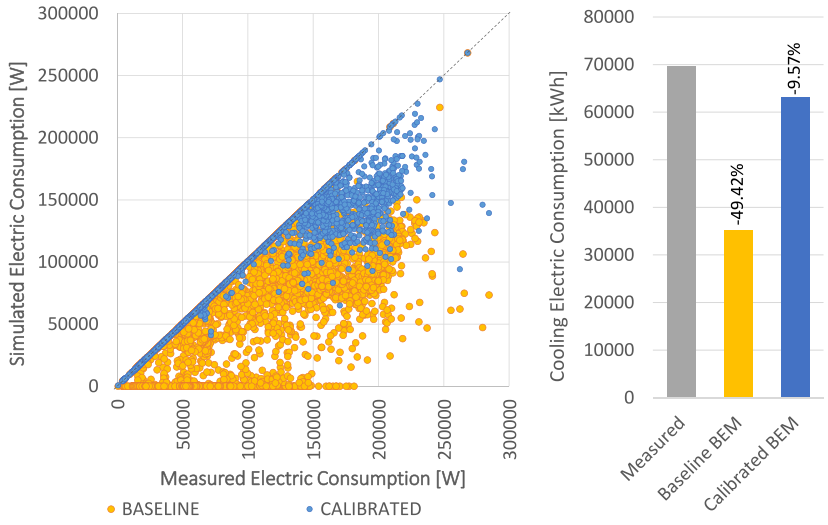

Fig. 9. Performance results for cooling consumption (district cooling usage) of the calibrated BEM during the cooling calibration period from June 2020 to the 15th of August 2020.

Table 13
Indoor temperature and cooling consumption hourly uncertainty index for the cooling calibration period using 985.16 h of operation from June 2020 to the 15th of August 2020.

Baseline BEM results						
Index	District cooling	Indoor temperatures				
		TZ-07	TZ-08	TZ-09	TZ-44	TZ-45
MAE	—	0.980	1.325	1.030	0.358	0.205
RMSE	—	1.221	1.665	1.316	0.450	0.256
NMBE	49.416%	−0.104%	1.443%	−1.698%	−1.111%	0.309%
Cv(RMSE)	69.236%	5.064%	6.733%	5.383%	1.895%	1.066%
R^2[a]	62.241%	40.703%	13.288%	56.438%	80.243%	86.179%
Calibrated BEM results						
Index	District cooling	Indoor temperatures				
		TZ-07	TZ-08	TZ-09	TZ-44	TZ-45
MAE	—	0.732	0.527	0.700	0.570	0.218
RMSE	—	0.956	0.689	0.902	0.727	0.271
NMBE	9.572%	−2.623%	−0.591%	−1.584%	−2.314%	0.216%
Cv(RMSE)	25.918%	3.967%	2.788%	3.689%	3.063%	1.129%
R^2[a]	90.926%	79.263%	81.569%	81.846%	71.742%	84.017%

[a]Although there is no universal standard for a minimum acceptable R^2 threshold, values above 75% are often considered a sign of a good causal relationship between the energy and independent variables [18].

the quality of information available on production units compared with terminal units, for which information is usually overlooked or less detailed. Additionally, the comparison validates the previous statement: the HP group requires fewer iterations than the distribution system to be calibrated.

However, as Table 13 shows, in terms of indoor climate, the calibration process improves the behavior of the showcase center (TZ-07, −08, and −09). Its goodness-of-fit index R^2 increased from values below 60% to values above the recommended 75%. The baseline BEM results are achieved by consuming only half of the cooling energy provided by the production units. In comparison, the calibrated model consumes most of the available cooling, reaching a Cv(RMSE) or 25.918% with an R^2 of 90.926%.

This calibration process executes energy redistribution through the different branches of the distribution system. Through the limitation of the maximum available energy, the HVAC parameters are adjusted by balancing the energy they demand with the temperature provided inside. The process depends on the quality of the objective function, and in this case a single objective function set was used (the weighted average by air volume of the building indoor temperature). This is the reason why the results displayed in Table 13 show that some thermal zones (TZ-44 and −45) may suffer a penalty in order to improve the behavior of the other building spaces.

It is to be noted that when assessing results regarding indoor temperatures where the expected band range of values is low (just a couple of Celsius degrees) in comparison to energy value ranges, meeting the goodness-of-fit index R^2 should be a requirement rather than a recommendation, especially since a shift in the residual of indoor temperature appears to have a huge impact on energy consumption.

4.3. Checking period results

The aim of the applied methodology is to achieve BEM calibration using shorter time periods than the yearly stream recommended by ASHRAE Guideline 14 [19]. Therefore, an evaluation period is required to check the overall BEM stability through time and avoid the model overfitting or overpredicting results. The selected verification period contains 690 h (around 70% the size of the training period) of previously unseen valid data running from the 16th of August through the

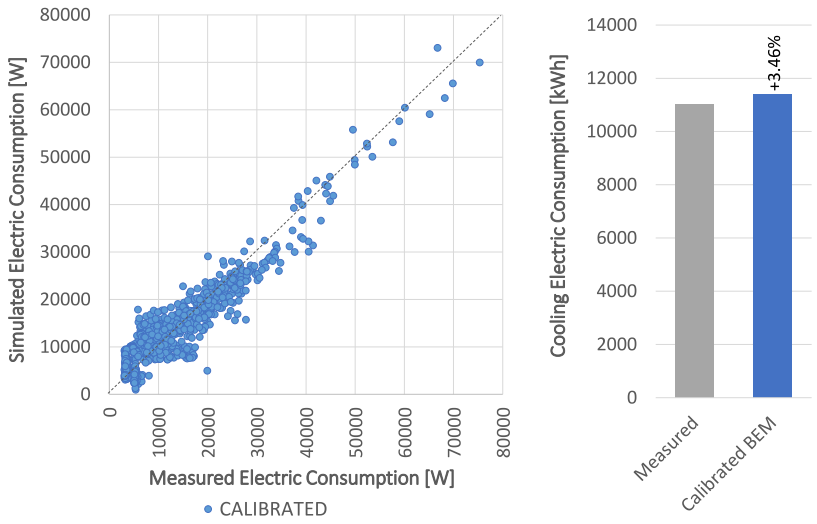

Fig. 10. Performance results for electric consumption of the HP group for the calibrated BEM during the validation period from the 16th of August 2020 to September 2020.

Table 14
On-site weather details for the summer verification period from 16th of August 2020 to September 2020. Table displays hourly maximum, average and minimum outdoor dry bulb temperature, and average global and diffuse radiation.

Description		Units	Checking period		
			Aug	Sep	Average
Outdoor	Average	°C	20.308	19.598	19.953
Dry Bulb	Maximum	°C	37.900	37.500	37.700
Temperature	Minimum	°C	11.900	9.500	10.700
Global Radiation	Average	W/m^2	372.530	259.715	316.122
Diffuse Radiation	Average	W/m^2	34.015	22.227	28.121

Table 15
Electric consumption hourly uncertainty index for the cooling evaluation period using 690 h of operation from 16th of August 2020 to September 2020.

Hourly index	ASHRAE	IPMVP	Electric consumption
NMBE	±10%	±5%	−3.459%
Cv(RMSE)	30%	20%	25.849%
R^2	75%	75%	89.621%

whole month of September in order to stress the calibrated BEM and assess its behavior.

In terms of outdoor conditions, this period is slightly cooler than the training period, with a monthly average temperature of 19.953 °C with maximum temperatures never exceeding 40 °C, as can be seen in Table 14.

Fig. 10 shows the dispersion of hourly electric consumption of the HP group, where the hourly points for simulated electric energy remain clustered around the ideal 45° line, whereas the overall energy consumption for the period is just 3.46% higher than the one measured for the equipment. The results shown in Table 15 indicate that the calibration for the HP group is stable through the rest of the summer 2020, with a CV(RMSE) of 25.84% and maintaining a goodness-of-fit R^2 above 75%.

In terms of the demand side terminal units, the results shown in Table 16 demonstrate that indoor temperatures are still within international standards. The HVAC systems make use of 85.11% of the available cooling energy provided by the HP group through the district cooling element in the simulation environment. Because the evaluation period uses previously unseen data, a reduction in the quality of the results is expected: in this case, there is an increase in the cooling energy NMBE from 9.57% to 14.89%, and yet the Cv(RMSE) and R^2 remain within international standards.

5. Conclusions

In the present study, we focused on calibration of the cooling system of multiple thermal zones in terms of indoor temperature and energy consumption during summer 2020. This procedure was reliant on minimum sensor deployment and the use of load profile/district cooling objects as a pivot to surpass the challenge posed in distributing cooling demand across building spaces. The result is a building energy model that describes the indoor thermal behavior of the structure and its equipment energy consumption. The calibrated building energy model was shown to meet hourly international standards for heat pump group electric consumption and indoor temperatures during its calibration period, in which only 985 h of ten-minute time-step data were used, and the model proved stable during the validation period (following 690 h of operation).

The study managed to find a distribution of cooling energy to the different thermal zones showing promising results. By the use of the load profile/district cooling element as a link between the production units and the building spaces allowed surpassing the challenge of having a major uncertainty point in the distribution system, namely the water flow for each branch of the piping system. Follow up studies will continue to address this issue, commonly found in most buildings.

Regarding the heat pump production units, the process grouped the equipment performance curves in two: one for the master unit and the other for the remaining units. The resulting curves show there is a difference in performance for each of the units. This suggest that finer subdivision of these performance curves, for example assigning each heat pump its own set of curves, may increase the quality of the obtained results. Even though, this may also mean an increase in the solution search space and additional computing power.

Building energy models should be developed according to their purpose, and in this particular case, the baseline model used to obtain the electric consumption of the heat pump group was sufficient for monthly energy assessment and certification purposes. However, the application of energy conservation measures or the development of other energy efficiency strategies requires a model that captures the building's behavior and the performance of its cooling/heating systems in a finer hourly resolution.

Additionally, the comparison between the baseline and the calibrated building energy models shows that regardless of how robust the information from technical documentation and building documents

Table 16
Electric consumption hourly uncertainty index for the cooling evaluation period using 690 h of operation from 16th of August 2020 to September 2020.

Hourly index	CIBSE	District cooling	Indoor temperatures				
			TZ-07	TZ-08	TZ-09	TZ-44	TZ-45
MAE	2.000	—	0.457	0.361	0.564	0.310	0.235
RMSE	1.500	—	0.646	0.521	0.759	0.418	0.290
NMBE	—	14.890%	−1.204%	−0.215%	−1.613%	−0.475%	0.390%
Cv(RMSE)	—	22.327%	2.713%	2.148%	3.158%	1.732%	1.195%
R^2	75%	92.395%	83.645%	86.677%	85.715%	73.333%	88.830%

appears, the building energy model will always require calibration because of the inherent design gap between the nominal value of the parameters, the installed equipment, and its actual operation due to local weather conditions or site occupation changes.

Future studies should focus on developing new techniques to improve the obtained results while attempting to improve the level of detail of the building energy models. Moreover, they should focus on applying the methodology to other equipment configurations and different cooling/heating systems while testing the calibrated building energy models for enhanced capabilities, such as renewable energy penetration, demand response, fault detection diagnosis, or model predictive control.

Abbreviations

The following abbreviations are used in this manuscript:

AHU	Air handling unit
ASHRAE	American Society of Heating, Refrigerating and Air-Conditioning Engineers
BEM	Building energy model
BMS	Building management system
CIBSE	Chartered Institution of Building Services Engineers
Cv(RMSE)	Coefficient of variation of mean Square Error
DoE	Department of Energy
DHW	Domestic hot water
DR	Demand response
DX	Direct expansion
ECMs	Energy conservation measures
EU	European Union
FCU	Fan coil unit
FEMP	Federal Energy Management Program
HP	Heat pump
HPWH	Heat pump water heater
HVAC	Heating, Ventilation, and Air Conditioning
IEA	International Energy Agency
IPMVP	International Performance Measurement and Verification Protocol
M&V	Measuring and verification
MAE	Mean absolute error
MPC	Model predictive control
NMBE	Normalized mean bias error
NSGA-II	Non-dominated sorting genetic algorithm
R^2	Spearman's rank correlation coefficient square
RMSE	Root mean square error
Temp.	Temperature
TZ	Thermal zone
C_i	Equation coefficients
$\overline{m}$	The mean of on-site measured values
m_i	The on-site measured value
n	The number of data points
p	Value of 1 (according to BEM M&V methodology)
$\overline{s}$	The mean of simulated values
s_i	The simulated value
x	Indoor air temperature (°C—wet bulb)
y	Outdoor air temperature (°C—dry bulb)
z	Either cooling capacity or electric consumption performance

CRediT authorship contribution statement

José Eduardo Pachano: Conceptualization, Methodology, Software, Validation, Investigation, Writing – original draft. **Juan Carlos Saiz:** Data provider, Writing – review & editing. **Carlos Fernández Bandera:** Conceptualization, Methodology, Validation, Investigation, Writing – original draft, Resources, Writing – review & editing, Supervision, Project administration, Funding acquisition.

Declaration of competing interest

The authors declare that there is no conflict of interest.

Data availability

The authors do not have permission to share data.

Acknowledgments

We would like to thank Fundación Saltoki (Spain), for providing us with both the building documentation and the sensor data to perform the necessary tests for this paper. All authors have approved the final version of the manuscript.

Funding

The researchers Carlos Fernández Bandera, Jose Pachano and María Fernández-Vigil Iglesias have been funded by the European Regional Development Fund (ERDF) and the Government of Navarra, Spain under the project "From BIM to BEM: B&B" (ref. 0011-1365-2020-000227)

References

[1] T. Vandenbussche, Is the EU's building renovation wave'fit for 55'? EPC Policy Brief June 2021, 2021.
[2] A. Clerici, G. Alimonti, World energy resources, in: EPJ Web of Conferences, Vol. 98, EDP Sciences, 2015, p. 01001.
[3] H. Brugger, W. Eichhammer, N. Mikova, E. Dönitz, Energy efficiency vision 2050: How will new societal trends influence future energy demand in the European countries? Energy Policy 152 (2021) 112216.
[4] L. Belussi, B. Barozzi, A. Bellazzi, L. Danza, A. Devitofrancesco, C. Fanciulli, M. Ghellere, G. Guazzi, I. Meroni, F. Salamone, et al., A review of performance of zero energy buildings and energy efficiency solutions, J. Build. Eng. 25 (2019) 100772.
[5] Y. Lu, Z.A. Khan, M.S. Alvarez-Alvarado, Y. Zhang, Z. Huang, M. Imran, A critical review of sustainable energy policies for the promotion of renewable energy sources, Sustainability 12 (12) (2020) 5078.

[6] K. Gram-Hanssen, S. Georg, Energy performance gaps: promises, people, practices, Build. Res. Inf. 46 (1) (2018) 1–9.
[7] D. Mariano-Hernández, L. Hernández-Callejo, A. Zorita-Lamadrid, O. Duque-Pérez, F.S. García, A review of strategies for building energy management system: Model predictive control, demand side management, optimization, and fault detect & diagnosis, J. Build. Eng. 33 (2021) 101692.
[8] R. Escandón, F. Ascione, N. Bianco, G.M. Mauro, R. Suárez, J.J. Sendra, Thermal comfort prediction in a building category: Artificial neural network generation from calibrated models for a social housing stock in southern Europe, Appl. Therm. Eng. 150 (2019) 492–505.
[9] T. Hong, Y. Chen, X. Luo, N. Luo, S.H. Lee, Ten questions on urban building energy modeling, Build. Environ. 168 (2020) 106508.
[10] P. Raftery, M. Keane, J. O'Donnell, Calibrating whole building energy models: An evidence-based methodology, Energy Build. 43 (9) (2011) 2356–2364.
[11] S. Papadopoulos, C.E. Kontokosta, A. Vlachokostas, E. Azar, Rethinking HVAC temperature setpoints in commercial buildings: The potential for zero-cost energy savings and comfort improvement in different climates, Build. Environ. 155 (2019) 350–359.
[12] M. Hu, F. Xiao, J.B. Jørgensen, R. Li, Price-responsive model predictive control of floor heating systems for demand response using building thermal mass, Appl. Therm. Eng. 153 (2019) 316–329.
[13] C. Fernández Bandera, J. Pachano, J. Salom, A. Peppas, G. Ramos Ruiz, Photovoltaic plant optimization to leverage electric self consumption by harnessing building thermal mass, Sustainability 12 (2) (2020).
[14] M. Curtis, J. Torriti, S.T. Smith, A comparative analysis of building energy estimation methods in the context of demand response, Energy Build. 174 (2018) 13–25.
[15] G. Ramos Ruiz, E. Lucas Segarra, C. Fernández Bandera, Model predictive control optimization via genetic algorithm using a detailed building energy model, Energies 12 (1) (2019).
[16] Z. Shao, E. Gholamalizadeh, A. Boghosian, B. Askarian, Z. Liu, The chiller's electricity consumption simulation by considering the demand response program in power system, Appl. Therm. Eng. 149 (2019) 1114–1124.
[17] D. Coakley, P. Raftery, M. Keane, A review of methods to match building energy simulation models to measured data, Renew. Sustain. Energy Rev. 37 (2014) 123–141.
[18] IPMVP Committee, et al., International performance measurement and verification protocol: Concepts and options for determining energy and water savings, volume i, Technical Report, National Renewable Energy Lab., Golden, CO (US), 2001.
[19] ASHRAE, ASHRAE guideline 14-2002: measurement of energy and demand savings, ASHRAE Guide 8400 (2002) 1–165.
[20] The Chartered Institution of Building Services Engineers, Requirements to be met by calculation methods for the simulation of thermal-energy efficiency of buildings and building installations, Standard ISBN978-1-912034-76-5, The Chartered Institution of Building Services Engineers, 222 Balham High Road, London SW12 9BS, 2020.
[21] U. DOE, M&V Guidelines: Measurement and Verification for Federal Energy Projects Version 3.0, US Department of Energy, 2008.
[22] R. Escandón, R. Suárez, J.J. Sendra, On the assessment of the energy performance and environmental behaviour of social housing stock for the adjustment between simulated and measured data: The case of mild winters in the Mediterranean climate of southern Europe, Energy Build. 152 (2017) 418–433.
[23] G.R. Ruiz, C.F. Bandera, Analysis of uncertainty indices used for building envelope calibration, Appl. Energy 185 (2017) 82–94.
[24] G.R. Ruiz, C.F. Bandera, T.G.-A. Temes, A.S.-O. Gutierrez, Genetic algorithm for building envelope calibration, Appl. Energy 168 (2016) 691–705.
[25] Z. O'Neill, B. Eisenhower, Leveraging the analysis of parametric uncertainty for building energy model calibration, in: Building Simulation, Vol. 6, (4) Springer, 2013, pp. 365–377.
[26] J.J. Robertson, B.J. Polly, J.M. Collis, Reduced-order modeling and simulated annealing optimization for efficient residential building utility bill calibration, Appl. Energy 148 (2015) 169–177.
[27] G.L. Martin, D. Monfet, H.F. Nouanegue, K. Lavigne, S. Sansregret, Energy calibration of HVAC sub-system model using sensitivity analysis and meta-heuristic optimization, Energy Build. 202 (2019) 109382.
[28] Y. Heo, R. Choudhary, G. Augenbroe, Calibration of building energy models for retrofit analysis under uncertainty, Energy Build. 47 (2012) 550–560.
[29] J. Yuan, V. Nian, B. Su, Q. Meng, A simultaneous calibration and parameter ranking method for building energy models, Appl. Energy 206 (2017) 657–666.
[30] A. Chong, K. Menberg, Guidelines for the Bayesian calibration of building energy models, Energy Build. 174 (2018) 527–547.
[31] A. Chong, K.P. Lam, M. Pozzi, J. Yang, Bayesian calibration of building energy models with large datasets, Energy Build. 154 (2017) 343–355.
[32] H. Lim, Z.J. Zhai, Influences of energy data on Bayesian calibration of building energy model, Appl. Energy 231 (2018) 686–698.
[33] V.G. González, L.Á. Colmenares, J.F.L. Fidalgo, G.R. Ruiz, C.F. Bandera, Uncertainy's indices assessment for calibrated energy models, Energies 12 (11) (2019).
[34] M. Royapoor, T. Roskilly, Building model calibration using energy and environmental data, Energy Build. 94 (2015) 109–120.
[35] D. Coakley, P. Raftery, P. Molloy, Calibration of whole building energy simulation models: detailed case study of a naturally ventilated building using hourly measured data, in: First Building Simulation and Optimization Conference, Loughborough, 2012, pp. 57–64.
[36] S. Qiu, Z. Li, Z. Pang, W. Zhang, Z. Li, A quick auto-calibration approach based on normative energy models, Energy Build. 172 (2018) 35–46.
[37] M. Aftab, C. Chen, C.-K. Chau, T. Rahwan, Automatic HVAC control with real-time occupancy recognition and simulation-guided model predictive control in low-cost embedded system, Energy Build. 154 (2017) 141–156.
[38] J. Yuan, V. Nian, B. Su, Q. Meng, A simultaneous calibration and parameter ranking method for building energy models, Appl. Energy 206 (2017) 657–666.
[39] D. Guyot, F. Giraud, F. Simon, D. Corgier, C. Marvillet, B. Tremeac, Building energy model calibration: A detailed case study using sub-hourly measured data, Energy Build. 223 (2020) 110189.
[40] H. Torio, A. Angelotti, D. Schmidt, Exergy analysis of renewable energy-based climatisation systems for buildings: A critical view, Energy Build. 41 (3) (2009) 248–271.
[41] A. Entrop, H. Brouwers, ECBCS Annex 49.
[42] C. Cornaro, F. Bosco, M. Lauria, V.A. Puggioni, L. De Santoli, Effectiveness of automatic and manual calibration of an office building energy model, Appl. Sci. 9 (10) (2019).
[43] B. Merema, M. Delwati, M. Sourbron, H. Breesch, Calibration of a BES model of an educational building with demand controlled ventilation, in: 15th Conference of IBPSA 43, Vol. 51, 2017.
[44] A. Cacabelos, P. Eguía, L. Febrero, E. Granada, Development of a new multi-stage building energy model calibration methodology and validation in a public library, Energy Build. 146 (2017) 182–199.
[45] D. Kim, S.J. Cox, H. Cho, P. Im, Model calibration of a variable refrigerant flow system with a dedicated outdoor air system: A case study, Energy Build. 158 (2018) 884–896.
[46] K. Subbarao, S. Didwania, T.A. Reddy, M. Addison, The enhanced parameter estimation (EPE) – a new calibration methodology for building energy simulations, 2021, arXiv:2103.07283.
[47] F. Tüysüz, H. Sözer, Calibrating the building energy model with the short term monitored data: A case study of a large-scale residential building, Energy Build. 224 (2020) 110207.
[48] M. Hydeman, K.L. Gillespie, A. Dexter, Tools and techniques to calibrate electric chiller component models, ASHRAE Trans. 108 (1) (2002) 733–741.
[49] J. Stein, M.M. Hydeman, Development and testing of the characteristic curve fan model, ASHRAE Trans. 110 (1) (2004).
[50] R. Yin, S. Kiliccote, M.A. Piette, Linking measurements and models in commercial buildings: A case study for model calibration and demand response strategy evaluation, Energy Build. 124 (2016) 222–235.
[51] J. Chen, X. Gao, Y. Hu, Z. Zeng, Y. Liu, A meta-model-based optimization approach for fast and reliable calibration of building energy models, Energy 188 (2019) 116046.
[52] T. Hong, J. Kim, J. Jeong, M. Lee, C. Ji, Automatic calibration model of a building energy simulation using optimization algorithm, Energy Procedia 105 (2017) 3698–3704, 8th International Conference on Applied Energy, ICAE2016, 8-11 October 2016, Beijing, China.
[53] J.E. Pachano, C.F. Bandera, Multi-step building energy model calibration process based on measured data, Energy Build. (2021) 111380.
[54] M. Mork, A. Xhonneux, D. Müller, Nonlinear distributed model predictive control for multi-zone building energy systems, Energy Build. 264 (2022) 112066.
[55] G. Serale, M. Fiorentini, A. Capozzoli, D. Bernardini, A. Bemporad, Model predictive control (MPC) for enhancing building and HVAC system energy efficiency: Problem formulation, applications and opportunities, Energies 11 (3) (2018).
[56] V. Gutiérrez González, G. Ramos Ruiz, C. Fernández Bandera, Empirical and comparative validation for a building energy model calibration methodology, Sensors 20 (17) (2020) 5003.
[57] U. DoE, Energyplus engineering reference, in: The Reference to Energyplus Calculations, 2010.
[58] Y. Zhang, I. Korolija, Performing complex parametric simulations with jeplus, in: SET2010-9th International Conference on Sustainable Energy Technologies, 2010, pp. 24–27.
[59] K. Deb, A. Pratap, S. Agarwal, T. Meyarivan, A fast and elitist multiobjective genetic algorithm: NSGA-II, IEEE Trans. Evol. Comput. 6 (2) (2002) 182–197.
[60] VDI-Fachbereich Technische Gebäudeausrüstung, Requirements to be met by calculation methods for the simulation of thermal-energy efficiency of buildings and building installations, Standard DINGCD22, Verlag des Vereins Deutscher Ingenieure, VDI - Platz 1, Düsseldorf, 40468 Germany, 2001.
[61] V.G. González, L.Á. Colmenares, J.F.L. Fidalgo, G.R. Ruiz, C.F. Bandera, Uncertainy's indices assessment for calibrated energy models, Energies 12 (11) (2019) 2096.
[62] C. Beck, J. Grieser, M. Kottek, F. Rubel, B. Rudolf, Characterizing global climate change by means of Köppen climate classification, Klimastatusbericht 51 (2005) 139–149.
[63] E. Lucas Segarra, H. Du, G. Ramos Ruiz, C. Fernández Bandera, Methodology for the quantification of the impact of weather forecasts in predictive simulation models, Energies 12 (7) (2019) 1309.

[64] G. Ramos Ruiz, E. Lucas Segarra, C. Fernández Bandera, Model predictive control optimization via genetic algorithm using a detailed building energy model, Energies 12 (1) (2019) 34.
[65] E. Lucas Segarra, G. Ramos Ruiz, C. Fernández Bandera, Probabilistic load forecasting for building energy models, Sensors 20 (22) (2020) 6525.
[66] H. Lim, Z.J. Zhai, Comprehensive evaluation of the influence of meta-models on Bayesian calibration, Energy Build. 155 (2017) 66–75.
[67] AHRI Air-Conditioning, Heating and Refrigeration Institute, Performance rating of central station air-handling units, Standard 430, AHRI Air-Conditioning, Heating and Refrigeration Institute, 2111 Wilson Boulevard Suite 500, Arlington, VA 22201, USA, 2009.
[68] Z. Yang, B. Becerik-Gerber, A model calibration framework for simultaneous multi-level building energy simulation, Appl. Energy 149 (2015) 415–431.
[69] D. Zhou, S.H. Park, Simulation-assisted management and control over building energy efficiency–a case study, Energy Procedia 14 (2012) 592–600.
[70] Y. Pan, Z. Huang, G. Wu, Calibrated building energy simulation and its application in a high-rise commercial building in shanghai, Energy Build. 39 (6) (2007) 651–657.
[71] D. Coakley, P. Raftery, P. Molloy, G. White, Calibration of a detailed BES model to measured data using an evidence-based analytical optimisation approach, in: Proceedings of Building Simulation 2011, 2011.
[72] Y.-S. Kim, M. Heidarinejad, M. Dahlhausen, J. Srebric, Building energy model calibration with schedules derived from electricity use data, Appl. Energy 190 (2017) 997–1007.